

The Globular Cluster System of the Spiral Galaxy NGC 7814

Katherine L. Rhode¹

Department of Astronomy, Yale University, New Haven, CT 06520

`rhode@astro.yale.edu`

Stephen E. Zepf

Department of Physics & Astronomy, Michigan State University, East Lansing, MI 48824

`zepf@pa.msu.edu`

ABSTRACT

We present the results of a wide-field photometric study of the globular cluster (GC) system of the edge-on Sab spiral NGC 7814. This is the first spiral to be fully analyzed from our survey of the GC systems of a large sample of galaxies beyond the Local Group. NGC 7814 is of particular interest because a previous study estimated that it has 500–1000 GCs, giving it the largest specific frequency (S_N) known for a spiral. Understanding this galaxy’s GC system is important in terms of our understanding of the GC populations of spirals in general and has implications for the formation of massive galaxies. We observed the galaxy in BVR filters with the WIYN 3.5-m telescope, and used image classification and three-color photometry to select GC candidates. We also analyzed archival HST WFPC2 images of NGC 7814, both to help quantify the contamination level of the WIYN GC candidate list and to detect GCs in the inner part of the galaxy halo. Combining HST data with high-quality ground-based images allows us to trace the entire radial extent of this galaxy’s GC system and determine the total number of GCs directly through observation. We find that rather than being an especially high- S_N spiral, NGC 7814 has $\lesssim 200$ GCs and $S_N \sim 1$, making it comparable to the two most well-studied spirals, the Milky Way and M31. We explore the implications of these results for models of the formation of galaxies and their GC systems. The initial results from our survey suggest that the GC systems of typical ellipticals can be accounted for by the merger of two or more spirals, but that for highly-luminous ellipticals, additional physical processes may be needed.

Subject headings: galaxies: individual (NGC 7814); galaxies: star clusters; galaxies: spiral

¹NASA Graduate Student Researchers Program Fellow

1. Introduction

Globular clusters (GCs) — with their old ages, extended spatial distributions and uniform chemical compositions — are powerful tools with which to study the formation of galaxies. Since the late 1980s, the study of GC systems of external galaxies has developed into a full-fledged subfield of astronomy (see Ashman & Zepf 1998, Harris 2001), with most of the emphasis placed on using GCs to piece together the dynamical and chemical enrichment history of giant galaxies. Much of the observational effort has focused on the GC systems of elliptical galaxies, including detailed investigations of their inner regions with the Hubble Space Telescope (e.g., Kundu & Whitmore 2001, Larsen et al. 2001) and some new wide-field studies using mosaic CCD detectors on ground-based telescopes (Rhode & Zepf 2001; Dirsch et al. 2003). But studies of the GC systems of spirals beyond the Local Group have lagged considerably behind those of ellipticals. A few HST studies of spirals have been done (Kissler-Patig et al. 1999, Goudfrooij et al. 2003), but their limited spatial extent prevents them from addressing the global properties of the galaxies' GC systems. Most previous ground-based studies were carried out many years ago using either small-format CCDs or photographic plates.

As a result, fundamental issues remain about the comparison between the GC systems of spirals and ellipticals, due in large part to the fact that our knowledge of spiral galaxy GC systems depends almost solely on the Milky Way and M31. For example, although there is reasonable evidence that elliptical galaxies in general have more GCs per unit mass than spirals, how large this difference is and how it depends on properties like morphological type and environment of the host galaxy are uncertain (see, e.g., Ashman & Zepf 1998, Kissler-Patig, Forbes, & Minniti 1998). The question of why ellipticals have more GCs per unit mass or luminosity than spirals has motivated much of the work in this field, but further progress depends on establishing the detailed properties of the GC systems of *both* ellipticals and spirals.

In an attempt to remedy some of the weaknesses in the census of spiral GC systems, we are carrying out a wide-field survey of the GCs around a good-sized sample of spirals beyond the Local Group. Our overall objectives are to expand the database of well-studied spirals and to use the information we gather to gain insight into how galaxies form. One specific aim is to test the predictions of formation scenarios for ellipticals. For example, prompted in part by evidence that elliptical GC systems are more populous and have higher mean metallicity than those of spirals, Ashman & Zepf (1992; hereafter AZ92) suggested that ellipticals form via mergers of two or more disk galaxies and that GCs are formed in these mergers. One of the predictions of AZ92 is that if Es form in galaxy mergers, they should have GC systems with bimodal color distributions; this was later confirmed by observations (e.g., Zepf & Ashman 1993, Gebhardt & Kissler-Patig 1999, Kundu & Whitmore 2001, Larsen et al. 2001). Another consequence of the AZ92 model is that the mass-normalized number of blue, metal-poor GCs in spiral galaxies should be the same as in ellipticals. This is because the blue, metal-poor GC population comes directly from the progenitor disk galaxies and the red, metal-rich GCs are formed in the merger. More broadly, any difference in the number of metal-poor GCs as a function of galaxy type or environment would provide important

clues to differences in the physical conditions in galaxies at early stages of their formation. These ideas can only be tested by establishing what these numbers are for a sample of spirals of different types.

Accordingly, we have obtained imaging data in three broadband filters for nine spiral galaxies, ranging in morphological type from Sab to Sc. All the targets are close to edge-on (with inclinations $\lesssim 80$ degrees) so that the GCs can be more easily detected, and all have distances of 20 Mpc or less. Most have data available in the HST archive, which we use to help characterize background galaxy contamination in the GC samples. As part of the same survey, we have also observed a sample of early-type galaxies out to large galactocentric radii in order to better constrain their GC system properties. A brief description of the overall study (ellipticals and spirals) is given in Rhode & Zepf (2001; Paper I).

We chose to begin our investigation of spirals with the Sab spiral NGC 7814. This galaxy was studied by Bothun, Harris, & Hesser (1992; hereafter B92), who detected ~ 120 GC candidates and estimated that the total number around the galaxy is ~ 500 –1000. B92 calculated a final specific frequency (S_N , the total number of GCs per unit luminosity of the host galaxy in units of $M_V = 15$) between 5.2 ± 2.2 and 7.6 ± 3.2 , depending on the assumed distance to NGC 7814. These are very large numbers compared to the Milky Way and M31, which have $S_N \sim 0.5$ –0.7 and 0.9–1.3, respectively (Ashman & Zepf 1998; Barmby 2003), and make NGC 7814 an obvious candidate for further study.

Here we present our findings for the GC system of NGC 7814. The next section describes our observations and initial data reduction steps. Section 3 describes the analysis of both the ground-based and HST data, and Section 4 gives the results. The paper ends with a discussion and summary of our results and their implications for spiral galaxy GC systems and galaxy formation models.

2. Observations and Initial Reductions

Images of NGC 7814 were obtained in 1998 December and 1999 October with the 3.5 m WIYN telescope² at Kitt Peak National Observatory. The detector used was a 2048x2048 CCD (S2KB), which has $0.196''$ -pixels and a field-of-view $6.7''$ on a side when mounted on WIYN. To observe as much of the galaxy halo and GC system as possible, we positioned the center of NGC 7814 in one corner of the CCD, which gives us radial coverage to $\sim 9'$, or ~ 35 kpc. To help separate *bona fide* GCs from contaminating objects (foreground stars and background galaxies), images were obtained in three broadband filters (BVR). Multiple exposures were taken in each filter and the telescope was dithered between exposures to facilitate cosmic ray removal. Total integration times were 7200 s

²The WIYN Observatory is a joint facility of the University of Wisconsin, Indiana University, Yale University, and the National Optical Astronomy Observatory.

(four exposures) in B , 5400 s (three exposures) in V and 5400 s (three exposures) in R . One B -band, one V -band, and the three R -band frames were taken under photometric conditions, and the rest of the images were taken on mostly clear, but not photometric, nights. Standard star fields (Landolt 1992) were observed during one night in 1999 October for use in the photometric calibration. The errors on the zero-point constants ranged from 0.003 to 0.005 magnitudes, indicating that the night was indeed photometric.

Preliminary reductions (overscan and bias level subtraction, flat-field division) of the WIYN images were accomplished using standard IRAF³ tasks. Sky subtraction was performed on the individual images taken in each filter before they were scaled to a common flux level and combined. The background level was restored to the combined images and they were aligned and flipped to a north-up, east-left orientation. The resolution (point-spread function FWHM) of the combined images is 1.0" in B , 1.0" in V , and 1.3" in R .

In addition to the WIYN data, we also made use of data from the HST archive⁴ for this study. Two Wide-Field and Planetary Camera 2 (WFPC2) data sets were available in the archive. Images from program GO.8597 (PI: Regan) were positioned with the center of the galaxy on the PC chip, and images from program GO.6685 (PI: Huizinga) were positioned away from the galaxy center, to include more of the halo. The former, which we will call the galaxy pointing, consisted of two exposures in the F606W filter of length 160 s and 400 s. The latter data set, hereafter referred to as the halo pointing, consisted of two 400 s frames in F450W, one 600 s frame in F555W, and one 600 s frame in F814W. “On-the-fly” calibration was applied to the data sets when we requested them from the archive. Multiple images of a given pointing taken in the same filter were combined using the STSDAS task CRREJ. The HST data were used to help quantify the contamination level of the WIYN data, as well as to find GCs in regions close to the galaxy disk; further analysis of the HST images is described in Sections 3.6 and 3.8.

3. Data Analysis

The techniques we use to detect, select, and analyze GC candidates around our target galaxies are explained in detail in Paper I. Here we describe the basic analysis steps for NGC 7814; the reader should consult Paper I for additional information.

³IRAF is distributed by the National Optical Astronomy Observatories, which are operated by AURA, under cooperative agreement with the National Science Foundation.

⁴Based on observations made with the NASA/ESA *Hubble Space Telescope*, obtained from the data archive at the Space Telescope Science Institute. STScI is operated by AURA, under NASA contract NAS 5-26555.

3.1. Source Detection

To remove the diffuse galaxy light and detect discrete sources around NGC 7814, the WIYN images were first smoothed with a circular median filter with a diameter 7 times the mean FWHM of point sources in the image. The smoothed image was subtracted from the original and a constant sky level was added to restore the background. The IRAF task DAOFIND was used to detect sources above a given signal-to-noise threshold in the galaxy-subtracted image. A total of 398 objects were detected that appear in all three filters.

3.2. Extended Source Cut

An extended source cut was applied to the WIYN source list in order to remove as many background galaxies as possible from the GC candidate list. The quality of the B and V -band images was significantly better than that of the R image, so the latter was not used for this step. The FWHM values of the 398 detected sources were measured in the B and V images and plotted versus their instrumental magnitudes. Figure 1 shows FWHM versus instrumental magnitude for the 398 objects in the B and V images, with filled circles indicating objects that met our selection criteria for point sources and open circles marking objects that were deemed extended and thus eliminated. As with NGC 4472 (Paper I), the HST images were used to fine-tune the extended source cut at the faint end. We eliminated 228 objects that were extended in either the B or V frames, leaving 170 apparent point sources in the WIYN images. This is a relatively large proportion of extended objects (60%); only 20% of the sources were extended in the NGC 4472 study. Indeed, upon examination this excess of extended objects is immediately apparent in the WIYN images: there are a large number of faint background galaxies across the entire frame, forming what looks like a cluster or group of galaxies behind NGC 7814.

3.3. Photometry

Sixteen standard stars from four Landolt fields observed during the photometric night in 1999 October were used to derive photometric calibration coefficients (zero points and color terms). Photometry in an aperture of radius equal to the mean FWHM of the image was carried out in B , V , and R on the 170 objects that passed the extended source cut. Calibrated total magnitudes were then calculated using aperture corrections and the photometric coefficients. The aperture corrections, which were derived in the same manner as for Paper I, are listed in Table 1. A galactic extinction correction, taken from the reddening maps of Schlegel, Finkbeiner, & Davis (1998), was applied to the final magnitudes; the corrections in the direction of NGC 7814 are $A_B = 0.194$, $A_V = 0.149$, and $A_R = 0.120$.

3.4. Color Selection

The final step in the GC candidate selection is to choose the subset of point sources with magnitudes and colors expected for GCs. We assumed that the brightest GC would have $M_V = -11$, based on the GCLF of the Milky Way and other galaxies (Ashman & Zepf 1998). The distance to NGC 7814 has recently been determined via the surface brightness fluctuation (SBF) technique by Tonry et al. (2001), who find $m - M = 30.60 \pm 0.14$. We adopt this distance for the rest of our calculations, unless noted otherwise. This yields an expected magnitude of $V = 19.6$ for the brightest GC around NGC 7814.

To select GC candidates by color, we used the McMaster catalog of Galactic GCs (Harris 1996) to derive a linear relationship between $B - V$ and $V - R$ color for GCs. We then chose a range of $B - V$ color for the selected GC candidates. The chosen range is 0.56 to 0.99, which corresponds to [Fe/H] between -2.5 and 0.0 for Galactic GCs. Our selection algorithm is as follows: objects with V fainter than 19.6 and photometric errors in all three filters of less than 0.15 mag were retained. Then, taking into account their individual photometric errors, objects with $B - V$ and $V - R$ that put them within 2.5-sigma of the derived relation for Galactic GCs were accepted as GC candidates. This yielded a list of 42 sources.

Figure 2 shows the results of the color selection. All 170 point sources in the WIYN image are plotted in the BVR color-color plane, with rejected objects as open squares and GC candidates as filled circles. For illustrative purposes, the locations of galaxies of various types are shown as “tracks” the galaxies would follow in the BVR plane with increasing redshift. Paper I describes how the tracks were produced. GCs coincide in the BVR plane with late-type, low- to moderate-redshift galaxies, some of which will have been eliminated from the GC sample by the extended source cut. Three-color photometry enables us to eliminate significant numbers of contaminating objects from the GC candidate list, but some contamination still remains. Section 3.6 describes how we quantify the contamination level.

3.5. Completeness Testing

A series of completeness tests was carried out to establish the point source detection limit in the WIYN images. Fifty artificial point sources with magnitudes within 0.1 magnitude of a given brightness were added to each image, the same detection steps used on the original image were performed, and the fraction of artificial sources detected was recorded. Fifty to sixty such tests were executed on each image so that the completeness was calculated over a range of 5 to 6 magnitudes per filter. The data are 50% complete at $B = 25.3$, $V = 24.8$, and $R = 23.9$.

3.6. Quantifying and Correcting for Contamination

3.6.1. Galaxies

HST resolves many faint background objects that can appear as point sources in ground-based images, so to estimate the galaxy contamination in the selected GC sample, we analyzed the archival HST data described in Section 2. Sixteen of the 42 WIYN GC candidates were located in at least one of the two HST pointings. We followed the method of Kundu et al. (1999) to determine which of these were true point sources. Photometry was performed with aperture radii of 0.5 pixels and 3 pixels and a sky annulus from 5 to 8 pixels. Objects in the PC chip with $\text{counts}_{3\text{pix}}/\text{counts}_{0.5\text{pix}} < 13$ and those in the WF chips with $\text{counts}_{3\text{pix}}/\text{counts}_{0.5\text{pix}} < 10$ were point sources and thus real GC candidates. Using these criteria (and confirming the results with visual inspection), we found that two of the 16 objects were actually galaxies.

To calculate the surface density of background galaxies in the GC sample, we first scaled the HST images to the same pixel scale as the WIYN images, aligned them to the WIYN pointing, and computed the total area covered by HST. The HST frames covered 4.41 square arc minutes around NGC 7814, yielding a density of 0.45 galaxies per square arc minute.

3.6.2. Stars

We used the latest version of the Galactic structure code from Mendez and van Altena (1996) and Mendez et al. (2000) to estimate the amount of stellar contamination in the GC sample. The model allows the user to choose such parameters as the contribution to star counts from the Galaxy disk, thick disk, and halo, and the galactocentric distance and z-height of the Sun. Output includes the surface density of stars expected within a given magnitude and color range in a given direction on the sky. A selection in two colors was not easily implemented so we used only a $B - V$ cut. The model predicts that in the direction of NGC 7814, the number density of stars with V magnitude and $B - V$ color in the range of our GC candidates is 0.11 stars per square arc minute. We varied the Galaxy parameters and the Sun’s location and found that the answer was the same each time. Applying both a $B - V$ and $V - R$ cut to our source list reduces the stellar contamination even more than selecting in just one color, so this is likely to be an overestimate of the stellar contamination.

3.6.3. Radially-Dependent Contamination Correction

The fraction of contaminating objects in the GC sample increases with radial distance as the GC surface density falls off. To determine exactly how the contamination fraction varies radially, the 42 GC candidates in the WIYN sample were assigned to annuli of width $1'$, starting at the galaxy center and continuing to $7'$. The number of non-GCs expected in each annulus was calculated by multiplying the number density of contaminating objects (0.56 per square arc minute) by the

effective area of the annulus (the portion where GCs could be detected; see Section 4.1). Finally, the contamination fraction in each annulus was calculated by dividing the number of contaminating objects by the number of GC candidates.

3.7. Determining the GCLF Coverage

An observed luminosity function (LF) was created by assigning the V magnitudes of the 42 WIYN GC candidates to 0.3-mag-wide bins. The radially-dependent contamination correction was applied to the LF data. The total completeness in each LF bin was calculated using the method described in Paper I (i.e., the completenesses in all three filters are convolved to come up with a total value), and the number of GCs in each bin was divided by the total completeness to produce a corrected LF.

The sample of 42 GC candidates is too small for use in determining NGC 7814’s intrinsic GCLF. Instead we assumed the GCLF was a Gaussian with a given peak magnitude and dispersion and fitted this to the data, varying only the normalization of the function. Based on the GCLF of the Milky Way, we used a peak magnitude of $M_V = -7.33$ (e.g., Ashman & Zepf 1998), which translates to $V = 23.27$ at the distance of NGC 7814. We fitted Gaussians with dispersions of 1.2, 1.3, and 1.4 magnitudes to the observed data. The fractional coverage fitting to the three Gaussians ranged from 0.41 to 0.46, with a mean value of 0.43 ± 0.02 .

Because there were so few GC candidates and we were fitting the LF data in the form of a histogram, we investigated the effect of the bin size on the fitting results. Changing the bin size can change the calculated fractional coverage by up to 4 percent. In Section 4.2 we quantify the effect of this and other uncertainties on the final numbers for NGC 7814’s GC system.

3.8. HST Sources in the Galaxy Disk and Inner Halo

The HST halo pointing was observed in three filters and was therefore useful for detecting GCs independently from the ground-based data. This provides a check on the WIYN results and gives radial coverage into the galaxy disk, where better resolution is especially useful for finding GCs. The halo pointing covers part of the disk and extends $\sim 2\text{--}3'$ into the halo.

GC candidates were located in the F555W and F814W images of the halo pointing using the method described in Kundu et al. (1999). DAOFLIND was used to detect sources above a modest threshold (3 counts above the background). Aperture photometry was then performed on each detected source and a signal-to-noise ratio (SNR) was computed using the counts in the aperture and the RMS scatter of the background. A total of 169 point-like objects were selected that had $\text{SNR} > 2.5$ in both images. Aperture photometry at the locations of the 169 sources was performed in all three filters using radii of 3 pixels for the PC chip and 2 for the WF chips and background

annuli from 5 to 8 pixels. Zero-points and aperture corrections for GCs at the distance of NGC 7814 were adopted from Kundu & Whitmore (2001) to calculate B , V , and I magnitudes for each object.

To construct a sample of GC candidates, sources with V magnitudes between 19.6 and 23.8 were selected. The faint magnitude cut was applied so the HST source list would be of similar depth to the WIYN list. It also eliminates the need for contamination corrections to the HST sample, since for magnitudes brighter than $V \sim 24$ the contamination level from background galaxies that would be unresolved in the HST images is negligible (Kundu et al. 1999). As before, we chose an acceptable $B - V$ range of 0.56 to 0.99 for GCs. Then we selected objects having $B - V$ and $V - I$ colors and photometric errors that put them within 3-sigma of the BVI color-color relation for Milky Way GCs. The slightly relaxed color criterion (3-sigma vs. 2.5 for the WIYN color selection) allowed for any differences between the HST and BVI filters. We also visually inspected each source; several that turned out to be diffuse knots of emission in the galaxy disk were eliminated. The final list of HST GC candidates includes 23 objects. Eleven of the objects also appeared in the WIYN list and the rest were not detected by WIYN, e.g., because they were in a masked region near the galaxy disk or were below the WIYN detection threshold. A color-magnitude diagram showing the V magnitudes and $B - V$ colors of all the GC candidates is shown in Figure 3.

Simulations following the method described in Kundu & Whitmore (2001) were run to establish the completeness level of the HST images. Briefly, a total of 70,000 artificial point sources with GC-like colors and a range of magnitudes were added to the V and I images and the detection steps described above were executed. The 50% completeness limits are $V = 25.1$ and $I = 24.1$.

The GCLF fitting and fractional coverage calculation were executed in the same way as for the WIYN sample. The resultant GCLF coverage ranged from 0.48 to 0.53, with a mean value of 0.51 ± 0.03 .

4. Results

4.1. Radial Distribution

To construct a radial distribution of GCs, the WIYN GC candidates were binned into annuli $1'$ wide, from the center of the galaxy out to $7'$. Portions of the WIYN images where GCs could not be reliably detected — namely, near the galaxy disk where the noise level is high and around bright stars where the CCD pixels are saturated — were masked out. An effective area was calculated for each annulus, which is equal to the area of the annulus minus the masked regions and the portion extending beyond the edges of the image.

The HST images used to detect GCs covered a smaller area around the galaxy than the WIYN frames, so to make full use of the data we binned the GCs into narrower annular regions. The 23 HST GC candidates were assigned to $0.5'$ -wide annuli from 0 to $2'$. A small portion of the images, coinciding with a dust lane in the galaxy disk, was masked out. Effective areas were calculated in

the same way as for the WIYN data.

To correct the WIYN data for contamination, the number density of contaminating stars and galaxies was subtracted from the number of GC candidates in each annulus. The contamination level in the HST sample was assumed to be insignificant, so no correction was applied. The number of GCs in each bin was then divided by the fractional GCLF coverage (0.43 for the WIYN data and 0.51 for the HST points). Finally, the radial profile was constructed by calculating a surface density of GCs for each annulus. The error on the surface density takes into account Poisson errors on the number of GCs and contaminating objects.

Because in some cases significant portions of the annuli were masked out or not observed (e.g., close to the galaxy disk and places where the annuli extend off the images), we calculated the mean distance of the unmasked pixels in each annulus and used that value to construct the profile. The profile is shown in Figure 4 and tabulated in Table 2. In the figure, filled circles are the WIYN points and open triangles are from HST. The top plot shows GC surface density versus radial distance in arc minutes and the bottom plot is the log of the surface density versus radius to the 1/4 power. The best-fit deVaucouleurs law is shown as a dashed line in the bottom plot and has the form $\log \sigma_{GC} = (2.86 \pm 0.46) - (1.81 \pm 0.44) r^{1/4}$, where σ_{GC} is the surface density of GCs in number per square arc minute and r is the projected radius. We also fitted a power law to the data; the best-fit line has the form $\log \sigma_{GC} = (1.03 \pm 0.06) - (0.98 \pm 0.25) \log r$. Both the deVaucouleurs law and power law fit the data fairly well inside 3', intersecting (or nearly intersecting) the data points plus error bars. Beyond 3', the deVaucouleurs law is a better match to the data; in this region, the points and error bars fall systematically below both of the fitted lines, but the discrepancy is not as large for the deVaucouleurs law.

For the 3–4' annulus and beyond, the GC surface density is consistent with zero within the errors. This result illustrates the importance of obtaining wide-field data when studying GC systems. The low values for the GC surface density at radii of 3' and beyond are critically important for constraining the total number of GCs around NGC 7814, since the inner points can be fit by many profiles that have quite different outer profiles and therefore total number. The observation of very low or zero GC surface density in the outer annuli strongly suggests that we have observed the entire radial extent of this galaxy's GC system. For the SBF distance modulus, 3' equals 11.5 kpc. For comparison, we note that if we projected the Milky Way's GC system onto the Y - Z plane (where Y is the Galactocentric coordinate in the direction of Galactic rotation and Z is the height above or below the plane) and calculated a radial distance for each GC, 82% of them would have radial distances of 11.5 kpc or less (Harris 1996).

4.2. Total Number and Specific Frequency

The information contained in the corrected GC radial profile can be used to calculate the total number of GCs around NGC 7814. Since we have combined HST data with wider-field WIYN data,

we can directly determine the total number of GCs without the extrapolation from smaller radius that would have been necessary had we used HST data alone. There are two ways to compute the total number: one is to integrate the best-fit deVaucouleurs profile from $r = 0$ to an outer radius, and the other is to sum the actual data points, i.e., by multiplying the surface density at each point in the profile by the area of the associated annulus and summing over all radii. Both methods produce a total number of GCs for the galaxy, corrected for magnitude incompleteness, missing spatial coverage, and contamination from non-GCs. The best-fit deVaucouleurs law provides a good fit to the radial profile data between $\sim 0.8'$ and $1.7'$, and either slightly or significantly overestimates the data elsewhere. For this reason we have used both methods — integrating the profile and summing the actual data — to calculate the total number of GCs in NGC 7814. Because the GC surface density is consistent with zero from $3'$ outward, and the deVaucouleurs function consistently overestimates the data points beyond that radius, we stop the integration or summation at that point. (Below we discuss the possible impact of our choice of integration limit on the final results.) Summing the data points in the profile to $3'$ yields a total of 140 GCs for NGC 7814. Integrating the best-fit deVaucouleurs law from 0 to $3'$ yields 190 GCs.

The total number of GCs can be normalized by luminosity or mass of the galaxy in order to facilitate comparison of NGC 7814's GC system to that of other galaxies. The specific frequency, S_N , is the number of GCs normalized by luminosity and is defined as

$$S_N \equiv N_{GC} 10^{+0.4(M_V + 15)} \quad (1)$$

(Harris & van den Bergh 1981). The total, extinction-corrected, face-on magnitude for NGC 7814 is $V_0^T = 10.20$ (RC3; deVaucouleurs et al. 1991). Since R_{25} for this galaxy is $2.75'$, virtually all of the galaxy light is located within $\sim 3'$. Therefore, integrating the GC profile to $3'$ and then using the total luminosity to calculate S_N is a reasonable approach. Assuming the SBF distance modulus yields a total absolute magnitude of $M_V^T = -20.40$. Combining this with the total numbers of GCs from summing the data or integrating the deVaucouleurs profile yields, respectively, $S_N = 1.0$ or 1.3.

The primary source of uncertainty on S_N is likely to be the galaxy magnitude, particularly since NGC 7814 is an edge-on spiral and correcting for extinction in such cases is difficult. The error on the total V magnitude quoted in RC3 is 0.13 mag, so M_V^T is at least that uncertain. If we assume that the actual total magnitude of NGC 7814 may be up to 0.3 mag brighter than the RC3 value, the result is a decrease in S_N of ~ 0.3 . Another source of uncertainty is associated with the GCLF coverage calculation. Depending on the dispersion assumed for the GCLF, the estimated coverage changed by as much as 5%. The coverage also varied by 4% depending on the bin size of the data. Taking both of these into account, the fractional coverage is known to $\sim 6\%$. This translates to an uncertainty in S_N of ~ 0.1 . The Poisson errors on the total numbers of GCs and contaminating objects results in an additional 0.1 uncertainty. Finally, there is uncertainty associated with the integration of the radial profile. One effect is that we stopped the integration at $3'$ (11.5 kpc), beyond which the GC surface density drops to zero. As mentioned, $\sim 18\%$ the Milky Way's GCs are located at radial distances beyond 11.5 kpc and it is possible that we have missed

some portion of NGC 7814’s GC system at these larger radii. Increasing the total number of GCs in NGC 7814 by 18% would increase S_N by ~ 0.2 . A second effect is that using a direct summation to $3'$ produces a S_N value 0.3 lower than integrating the de Vaucouleurs fit over the same region. If we combine the above sources of uncertainty on S_N in quadrature, we obtain a final value of S_N of 1.3 ± 0.4 for NGC 7814.

Normalizing the number of GCs by host galaxy mass makes it easier to compare the GC systems of galaxies with different star formation histories (such as spirals and ellipticals) and thus different mass-to-light ratios in their stellar populations. Zepf & Ashman (1993) suggest using a parameter called T , which they define as

$$T \equiv \frac{N_{GC}}{M_G/10^9 \text{ M}_\odot} \quad (2)$$

where N_{GC} is the number of GCs and M_G is the mass of the host galaxy. Following Zepf & Ashman (1993), we adopt a mass-to-light ratio $M/L_V = 6.1$ for an Sab spiral like NGC 7814. Combining this with $N_{GC} = 140$ yields $T = 1.9$, and using $N_{GC} = 190$ gives $T = 2.5$ for NGC 7814. The values derived for total number and specific frequency are summarized at the end of this section.

4.3. Mass-Normalized Number of Blue Globular Clusters

One of the main objectives of our overall study is to test a specific prediction of the AZ92 merger scenario for the origin of ellipticals. In this scenario, two (or more) disk galaxies with their own GC systems merge to form an elliptical. A metal-rich population of GCs forms from the colliding gas as the spirals merge. The metal-poor GCs in the progenitor spirals become the metal-poor population in the elliptical. The end result is an elliptical with bimodal color and metallicity distributions of GCs. As mentioned in the Introduction, a consequence of this scenario is that the mass-normalized number of metal-poor GCs in a typical spiral should be the same as in ellipticals. In this simple merger picture, the GCs created in the merger are formed from enriched gas (and are thus metal-rich), so even if a given elliptical has been formed from multiple disk galaxies, the mass-normalized number of metal-poor GCs (T for the metal-poor population, which we will refer to as T_{blue}) should stay fairly constant. We can directly test the AZ92 prediction by comparing T_{blue} for NGC 7814 (assuming it to be a typical Sab spiral) to typical T_{blue} values for ellipticals.

Table 3 shows that T for NGC 7814’s *entire* GC system is within the range 1.9 to 2.5. To determine T_{blue} we first need to select a subsample of GC candidates that is equally complete in all three filters. The reddest GC candidate in our list has $B - R = 1.64$. The GC list is 90% complete at $B = 24.3$, so to construct a “complete sample”, we cut the 42-candidate list at $R = 22.7$. This yields 21 objects. One of the objects is extended in the HST images, so this leaves 20 objects.

Given sufficient numbers of GC candidates, one can derive robust values for the relative proportions of red and blue GCs in a galaxy. This is typically done by fitting multiple Gaussian functions to a color distribution made with a complete sample, e.g., using the KMM algorithm

(Ashman, Bird, & Zepf 1994). We did this in Paper I using 366 GC candidates in NGC 4472 and found that the color distribution was significantly bimodal, with a gap between the blue and red populations at $B - R = 1.23$. The sample of 20 objects in NGC 7814 does not appear bimodal and is too small to use with KMM, which requires at least 50 objects to produce a reliable result. If we instead simply divide the sample in the way that NGC 4472’s GC population is divided (i.e., at $B - R = 1.23$), we find that eight GC candidates are blue and 12 are red. With such small numbers the uncertainties on the overall proportions of blue and red GCs in the system are large. Moreover, there are possible systematic errors in play: some of the GC candidates are likely reddened due to internal extinction in NGC 7814, in which case more may actually belong in the blue category. (In fact, six of the 13 GCs with $B - R > 1.23$ have radial distances within 2' of the center of NGC 7814, where the diffuse galaxy light is appreciable; reddening could very well be a factor for some of these objects.) Because of these uncertainties, we will adopt 40% as a *lower limit* on the percentage of blue GCs in the NGC 7814 system. Applying this percentage to $T = 2.5$ yields a mass-normalized number of blue GCs, T_{blue} , of 1.0.

Even if several of the GC candidates in the complete sample are affected by reddening, it is unlikely that *all* of them actually belong in the blue category. To estimate an upper limit for the proportion of blue GCs, we look at the most well-known spirals, the Milky Way and M31. About 70% of the GCs in the Milky Way are part of the metal-poor, “halo” population (Harris 1996; Côté 1999). The fraction is similar in M31, at 66% (Barmby et al. 2000). If we assume that the proportion of blue GCs in NGC 7814 is also $\sim 70\%$, and that the total T is 2.5, then T_{blue} for this galaxy is 1.8.

By the above arguments, T_{blue} for NGC 7814 is between ~ 1 and 2. We will compare this range of values to that of other galaxies and discuss the implications for galaxy formation in Section 5.

4.4. Effect of Change in Distance on Specific Frequency

Since distances to individual galaxies have some uncertainty, we have explored the effect of changing the galaxy distance on the total number and specific frequency of GCs. The SBF distance used in this paper ($m - M = 30.60 \pm 0.14$, or 13.2 Mpc) was only recently published (Tonry et al. 2001). Despite being an edge-on spiral, NGC 7814 does not have a published Tully-Fisher distance, so B92 used its radial velocity and a Virgocentric flow model to derive a distance of 12.5 Mpc ($m - M = 30.48$). They also calculated results using a distance modulus 1 mag further, based on the fact that their GCLF changed appreciably depending on whether they treated one of their observed fields as background or GC system.

To illustrate the effect of distance on the derived properties of NGC 7814’s GC system, we will adopt a distance modulus of 30.95, which is the SBF value plus 2.5σ . The larger distance increases the total number of GCs, primarily because the GCLF coverage is reduced, but the effect on S_N is counteracted by a brighter absolute magnitude for the galaxy. The luminosity- and mass-

normalized GC specific frequencies for NGC 7814 at this alternative distance are $S_N = 0.8$ and 1.0 (from summing the data and integrating the fit) and $T = 1.4$ and 1.9 (data and fit). Therefore, using a farther distance results in a slightly smaller specific frequency.

Table 3 lists the total numbers and specific frequencies for NGC 7814’s system for the two different distance moduli. Columns (1) and (2) give the assumed distance modulus and distance to the galaxy and column (3) the galaxy luminosity. Columns (4)–(6) are, respectively, the total number of GCs, the luminosity-normalized specific frequency S_N and the mass-normalized specific frequency T for the total system. The first number given in each of columns (4)–(6) comes from summing the data points in the radial profile and the second (larger) number from integrating the best-fit deVaucouleurs function.

5. Discussion

As stated in the Introduction, NGC 7814 was of particular interest to us as a possible example of a spiral galaxy with an extremely populous GC system. When we began our study, it was thought to have by far the largest GC specific frequency of any spiral (Harris 1991; Ashman & Zepf 1998). We find instead that NGC 7814 has $\lesssim 200$ GCs and $S_N \sim 1$. This makes it comparable to our own Galaxy, which has ~ 150 known GCs, an estimated total population of ~ 180 and $S_N \sim 0.5$ – 0.7 , and M31, with N_{GC} estimated at ~ 450 and $S_N \sim 0.9$ – 1.3 (Ashman & Zepf 1998; Barmby 2003).

In their study of NGC 7814, B92 detected ~ 120 GC candidates and, correcting for areal and magnitude incompleteness and extrapolating the radial profile to both smaller and larger radius, concluded that it had a GC system with 500–1000 GCs. They used the technology available at the time, namely a CCD with $0.4''$ -pixels, which made it more difficult to eliminate contaminating galaxies. Furthermore, they observed the galaxy in a single filter (V), so selecting GCs by color was not possible. They observed several fields around the galaxy to cover a substantial fraction of the GC system, as well as control fields away from the target to help correct for contamination. The latter should in theory work well, but as noted in Section 3.2 there appears (from our data) to be an overdensity of background galaxies in the direction of NGC 7814. If their control field did not have a correspondingly high density of background objects, they would have under-corrected for contamination, resulting in an overestimate of the number of GCs in NGC 7814. We note that for the Virgo elliptical NGC 4472, our techniques for reducing and correcting for contamination also resulted in a smaller S_N value (Paper I) than previous estimates.

A major objective of our GC system survey is to test whether the mass-normalized total numbers of metal-poor GCs in spirals and ellipticals are the same, as expected, for example, in the AZ92 merger model for the formation of ellipticals. The numbers of GCs in ellipticals vary with the luminosity of the host galaxy, with more luminous galaxies generally hosting larger populations of globulars (e.g., Harris & Racine 1979, Djorgovski & Santiago 1992, Zepf, Geisler, & Ashman 1994). Therefore to fully test the AZ92 picture we need to compare T_{blue} for spirals with ellipticals

of varying luminosities. As part of our survey, we are studying the total GC populations of a sample of early-type galaxies with a range of luminosities. An example of a modest-luminosity elliptical is NGC 3379, an E1 with $M_V \sim -21$. We find that this galaxy has ~ 270 GCs. Using the above V -band magnitude and a mass-to-light ratio M/L_V of 10 for ellipticals (Zepf & Ashman 1993), this translates to a total S_N of 1.2 and $T \sim 1.4$ (Rhode & Zepf, in preparation; Paper III). Approximately 70% of the GC candidates in NGC 3379 are blue, so $T_{\text{blue}} \sim 1$. By comparison, in Section 4.3 we estimated that T_{blue} for NGC 7814 is between 1 and 2. In the Milky Way and Andromeda, about 70% of the GCs are metal-poor, so for these galaxies T_{blue} is, respectively, ~ 0.9 and ~ 1.2 . These numbers indicate that it is possible to create the blue GC population of NGC 3379 simply by merging the GC systems of spirals like NGC 7814 or the Milky Way. Thus it appears that — in terms of the total numbers of GCs — a simple merger scenario can account for the GC system of a galaxy like NGC 3379 if one assumes, as AZ92 did, that the number of new GCs formed in the merger is roughly equal to the number originally contained in the spirals.

NGC 4472 is the brightest galaxy in Virgo (with $M_V \sim -23$) and is a good example of a giant cluster elliptical. In Paper I, we calculated a total number of GCs (~ 5900) and the proportions of red and blue GCs in NGC 4472 (40% and 60%, respectively). Again assuming a mass-to-light ratio M/L_V of 10, we derived $T = 2.6$ for the blue, metal-poor GC population of NGC 4472. While T_{blue} for NGC 7814 is larger than for the Milky Way and M31, at between ~ 1 and 2, it does not appear to be large enough to fully account for the large blue GC population in a galaxy like NGC 4472. In this case our data suggest that a simple merger scenario along the lines of AZ92 cannot explain how massive ellipticals like NGC 4472 and their GC systems formed.

To reiterate, the results from our study so far indicate that the metal-poor GC populations of modest-luminosity, low- S_N ellipticals can be accounted for by the merger of typical spirals, whereas T_{blue} for a luminous, high- S_N elliptical like NGC 4472 is larger than for any spiral studied to date. We note that other authors (e.g., Harris 1981; van den Bergh 1984; Harris 2001) have argued similarly, that the GC systems of giant cluster Es cannot have formed via simple spiral-spiral mergers. These previous arguments were typically based on comparisons of total S_N for spirals and ellipticals rather than the specific frequency of the blue GCs alone. A final effect that needs to be accounted for in our discussion of T is that mass-to-light ratios of ellipticals vary with galaxy luminosity. More luminous ellipticals are redder than lower-luminosity ones, and for all stellar populations models (e.g., Bruzual & Charlot 1993) this leads to higher stellar M/L_V for higher- L ellipticals. We will discuss the implications of this in more detail in Paper III. Models of this effect (e.g., Zepf & Silk 1996; see also Dressler et al. 1987) suggest that stellar population differences between ellipticals of different luminosities can account for up to about half of the increase in T with increasing elliptical galaxy luminosity. Thus, even with variations in M/L_V for ellipticals, there remain differences between T_{blue} for spirals (and low-luminosity Es) compared to luminous Es. This seems to suggest that GC systems form or evolve differently depending on the luminosity of the host galaxy.

One possibility is that the number of old, metal-poor GCs is higher in more luminous ellipticals

because there is less dynamical destruction of GCs in these galaxies compared to lower-luminosity ellipticals and spirals. Murali & Weinberg (1997a) modeled the evolution of the GC system of M87 and used scaling relations to translate their results to ellipticals of various luminosities. They suggest that ellipticals may have formed with similar GC specific frequencies but that GCs in lower-luminosity Es underwent more dynamical destruction due to their higher densities, resulting in a trend of higher S_N with higher galaxy luminosity. Similarly, Vesperini (2000) modeled GC destruction in ellipticals with a range of masses and found that the fraction of surviving clusters increases with increasing galaxy mass. With regard to spirals, simulations exploring the effect of dynamical destruction on GCs in the Milky Way system (e.g., Murali & Weinberg 1997b; Vesperini 1998) suggest that, just as in low-luminosity ellipticals, it is likely that a significant fraction of the population has been destroyed over a Hubble time. Therefore, while this is certainly not required to be the case, there remains the possibility that spirals at high redshift had large enough metal-poor GC populations to account for what we see in luminous ellipticals today.

Recent work on hierarchical merging scenarios for galaxy formation (e.g., Beasley et al. 2002, Santos 2003) provides another possible explanation for the apparent luminosity-dependence of T_{blue} . In these types of scenarios, metal-poor GCs are formed at high redshift in protogalactic fragments; the gas-rich fragments merge over time, producing metal-rich GCs and eventually resulting in the massive galaxies and GC systems that we see today. Santos (2003) proposes that metal-poor GC formation occurred at redshifts prior to $z \sim 7$ before being suppressed by reionization. In this picture, the timing of the collapse of structures in the pre-reionization Universe is what determines how many blue GCs are contained in a given end-product galaxy. Massive galaxies like giant cluster Es collapsed earlier, which means that a larger fraction of their eventual mass was in place by the time reionization occurred. Less massive galaxies like spirals and field galaxies collapsed later, so fewer blue GCs were produced in them before GC formation was halted. The natural result is that more massive (and thus more luminous) galaxies will have more blue, metal-poor GCs per unit mass than less massive objects. Within the framework of this scenario, the observed spatial distributions of the metal-poor GCs can help place constraints on the redshifts at which the protogalactic fragments collapsed, as well as on the masses of the fragments. In hierarchical models, the most overdense fragments that collapse at the highest redshifts (and can begin to form GCs) are more centrally-concentrated than those with lower densities that collapse later. Likewise, fragments with more mass will also collapse earlier and be more concentrated toward the galaxy center. Santos has simulated this in detail for the Milky Way GC system, but has not yet produced testable predictions for the GC spatial distributions of other galaxies. In future, however, our observed GC spatial profiles for galaxies with a variety of masses and in different environments will provide valuable constraints for this theoretical work.

6. Summary

We have undertaken a wide-field CCD survey of the GC systems of a large sample of spiral and elliptical galaxies with the primary goal of testing models for the origin of ellipticals, including the idea that they are formed via spiral-spiral mergers. We have completed our study of NGC 7814, an Sab spiral that was found in past work to have an extremely high GC specific frequency. Our main results are as follows:

1. Our data provide radial coverage of NGC 7814’s GC system to $\sim 7'$ (~ 30 kpc) from the galaxy center. The surface density in the radial distribution of GCs is consistent with zero by $\sim 3-4'$ ($\sim 11-15$ kpc) from the galaxy center, suggesting that we have observed the full extent of NGC 7814’s GC system.
2. NGC 7814 has a total population of ~ 200 GCs and a luminosity-normalized specific frequency S_N of 1.3 ± 0.4 . NGC 7814 is not a high- S_N spiral as previously claimed, but instead has a GC system that is comparable to those of the two most well-studied spirals, the Milky Way and M31.
3. A natural consequence of the fact that NGC 7814 has many fewer GCs than previously thought is that the number of metal-poor GCs must also be substantially reduced. We compare NGC 7814’s blue GC population to that of ellipticals from our study in order to test a prediction of the Ashman & Zepf merger model. We find that merging the blue GC populations of spirals like NGC 7814 is enough to account for the blue GCs in a moderate-luminosity field elliptical like NGC 3379, but not in a giant cluster elliptical like NGC 4472. This suggests that simple mergers may be able to explain the origins of typical-luminosity ellipticals but that some additional process is needed to account for the GC systems of more massive ellipticals.

Our findings for NGC 7814 significantly alter the overall picture of extragalactic GC systems. In Paper III of this series, we will present results for the remaining early-type galaxies in the sample and will specifically address predictions of the various scenarios for the formation of ellipticals, including (in addition to the merger model) multi-phase collapse (Forbes et al. 1997), collapse plus accretion (Côté et al. 1998), and hierarchical merging (e.g., Beasley et al. 2002, Santos 2003).

K.L.R. gratefully acknowledges financial support from a NASA Graduate Student Researchers Fellowship for this project. S.E.Z. acknowledges support for this work from the Michigan State University Foundation and NASA Long-Term Space Astrophysics Grant NAG5-11319. We are grateful to Arunav Kundu for his assistance with the HST data analysis, which included providing a list of detected objects in the HST halo pointing and running completeness tests on those data. We thank the staff at WIYN and Kitt Peak National Observatory for assistance during our observing runs. We also thank the anonymous referee for providing useful comments that improved the quality of the paper. This research has made use of the NASA/IPAC Extragalactic Database (NED), which is operated by the Jet Propulsion Laboratory, California Institute of Technology, under contract

with the National Aeronautics and Space Administration.

REFERENCES

Ashman, K.M., Bird, C.M., & Zepf, S.E. 1994, AJ, 108, 2348

Ashman, K.M., & Zepf, S.E. 1992, ApJ, 384, 50

Ashman, K.M., & Zepf, S.E. 1998, Globular Cluster Systems (Cambridge: Cambridge University Press)

Barmby, P. 2003, in Extragalactic Globular Cluster Systems, ed. M. Kissler-Patig (New York: Springer-Verlag)

Barmby, P., Huchra, J.P., Brodie, J.P., Forbes, D.A., Schroder, L.L., & Grillmair, C.J. 2000, AJ, 119, 727

Beasley, M.A., Baugh, C.M., Forbes, D.A., Sharples, R.M., & Frenk, C.S. 2002, MNRAS, 333, 383

Bothun, G.D., Harris, H.C., & Hesser, J.E. 1992, PASP, 104, 1220

Bruzual, A.G. & Charlot, S. 1993, ApJ, 405, 538

Coleman, G.D., Wu, C.-C., & Weedman, D.W. 1980, ApJS, 43, 393

Côté, P. 1999, AJ, 118, 406

Côté, P., Marzke, R.O., & West, M.J. 1998, ApJ, 501, 554

de Vaucouleurs, G., de Vaucouleurs, A., Corwin Jr., H.G., Buta, R.J., Paturel, G., & Fouque, P. 1991, Third Reference Catalogue of Bright Galaxies (New York: Springer)

Dirsch, B., Richtler, T., Geisler, D., & Forte, J.C., Bassino, L.P., & Gieren, W.P. 2003, AJ, 125, 1908

Djorgovski, S. & Santiago, B.X. 1992, ApJ, 391, L85

Dressler, A., Lynden-Bell, D., Burstein, D., Davies, R.L., Faber, S.M., Terlevich, R.J., & Wegner, G. 1987, ApJ, 313, 42

Forbes, D.A., Brodie, J.P., & Grillmair, C.J. 1997, AJ, 113, 1652

Gebhardt, K. & Kissler-Patig, M. 1999, AJ, 118, 1526

Goudfrooij, P., Strader, J., Brenneman, L., Kissler-Patig, M., Minniti, D., & Huiizing, E. 2003, MNRAS, in press

Harris, W.E. 1981, ApJ, 251, 497

Harris, W.E. 1991, ARA&A, 29, 543

Harris, W.E. 1996, AJ, 112, 1487

Harris, W.E. 2001, in Saas-Fee Advanced Course 28, Star Clusters, ed. L. Labhardt & B. Binggeli (Berling: Springer-Verlag), 223

Harris, W.E. & Racine, R. 1979, ARA&A, 17, 241

Harris, W.E. & van den Bergh, S. 1981, AJ, 86, 1627

Kennicutt, R.C. Jr. 1992, ApJS, 79, 255

Kinney, A.L., Calzetti, D., Bohlin, R.C., McQuade, K., Storchi-Bergmann, T., & Schmitt, H.R. 1996, ApJ, 467, 38

Kissler-Patig, M., Forbes, D.A., & Minniti, D. 1998, MNRAS, 298, 1123

Kissler-Patig, M., Ashman, K.M., Zepf, S.E., & Freeman, K.C. 1999, AJ, 118, 197

Kundu, A. & Whitmore, B.C. 2001, AJ, 121, 2950

Kundu, A., Whitmore, B.C., Sparks, W.B., & Macchetto, F.D. 1999, ApJ, 513, 733

Landolt, A.U. 1992, AJ, 104, 340

Larsen, S.S., Brodie, J.P., Huchra, J.P., Forbes, D.A., & Grillmair, C.J. 2001, AJ, 121, 2974

Mendez, R.A. & van Altena, W.F. 1996, AJ, 112, 655

Mendez, R.A., Platais, I., Girard, T.M., Kozhurina-Platais, V., & van Altena, W.F. 2000, AJ, 119, 813

Murali, C. & Weinberg, M.D. 1997a, MNRAS, 288, 767

Murali, C. & Weinberg, M.D. 1997b, MNRAS, 291, 717

Rhode, K.L. & Zepf, S.E. 2001, AJ, 121, 210

Santos, M.R. 2003, in Extragalactic Globular Cluster Systems, ed. M. Kissler-Patig (New York: Springer-Verlag)

Schlegel, D.J., Finkbeiner, D.P., & Davis, M. 1998, ApJ, 500, 525

Tonry, J.L., Blakeslee, J.P., Ajhar, E.A., Fletcher, A.B., Luppino, G.A., Metzger, M.R., & Moore, C.B. 2001, ApJ, 546, 681

van den Bergh, S. 1984, PASP, 96, 329

Vesperini, E. 1998, MNRAS, 299, 1019

Vesperini, E. 2000, MNRAS, 318, 841

Zepf, S.E., & Ashman, K.M. 1993, MNRAS, 264, 611

Zepf, S.E., Geisler, D., & Ashman, K.M. 1994, ApJ, 435, L117

Zepf, S.E. & Silk, J. 1996, ApJ, 466, 114

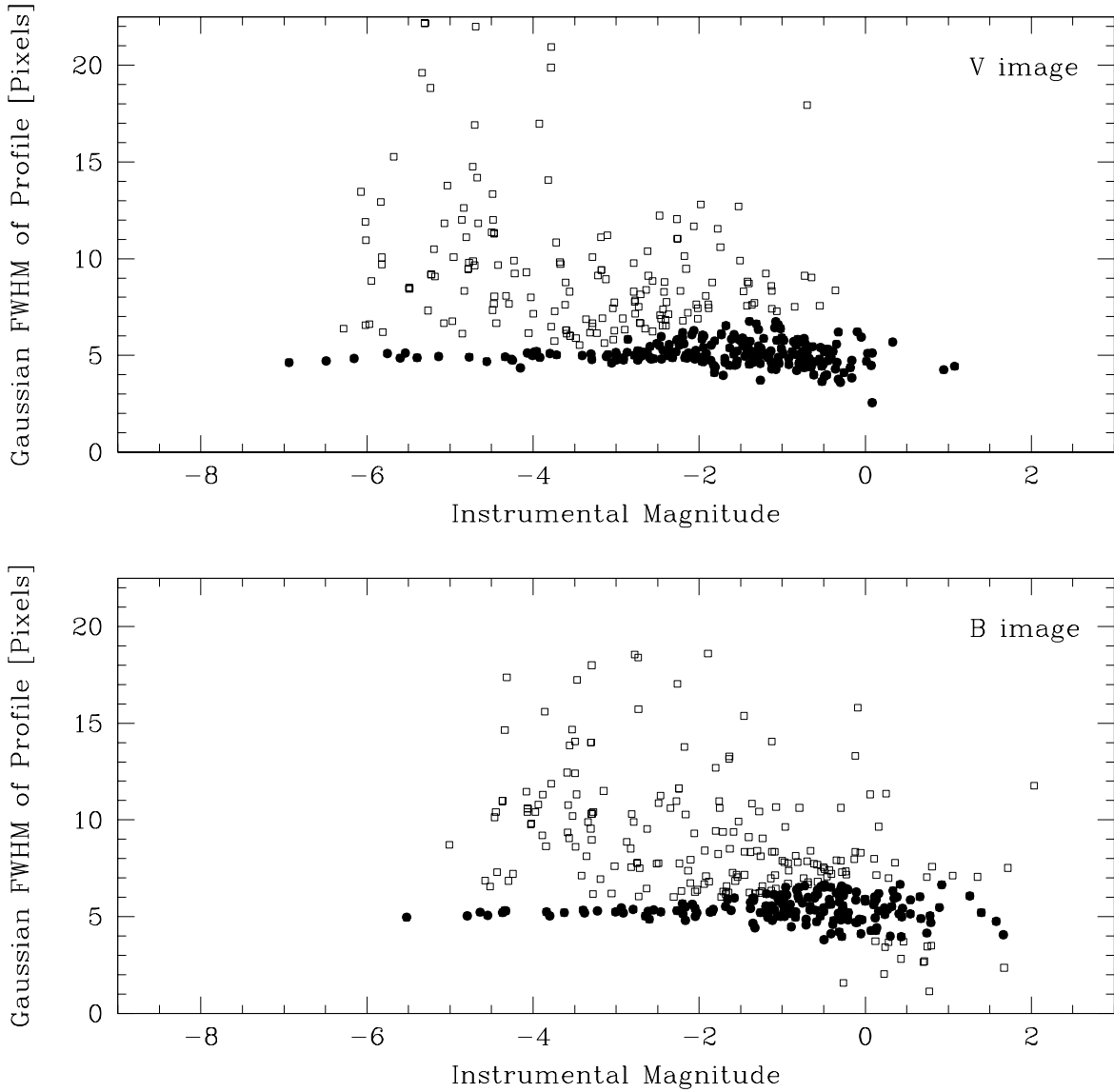


Fig. 1.— Gaussian FWHM of the radial profile versus instrumental magnitude for the 398 detected objects in the WIYN V and B images. Filled circles are objects that passed the extended source cut and open squares are objects deemed extended and therefore eliminated from the list of possible GCs.

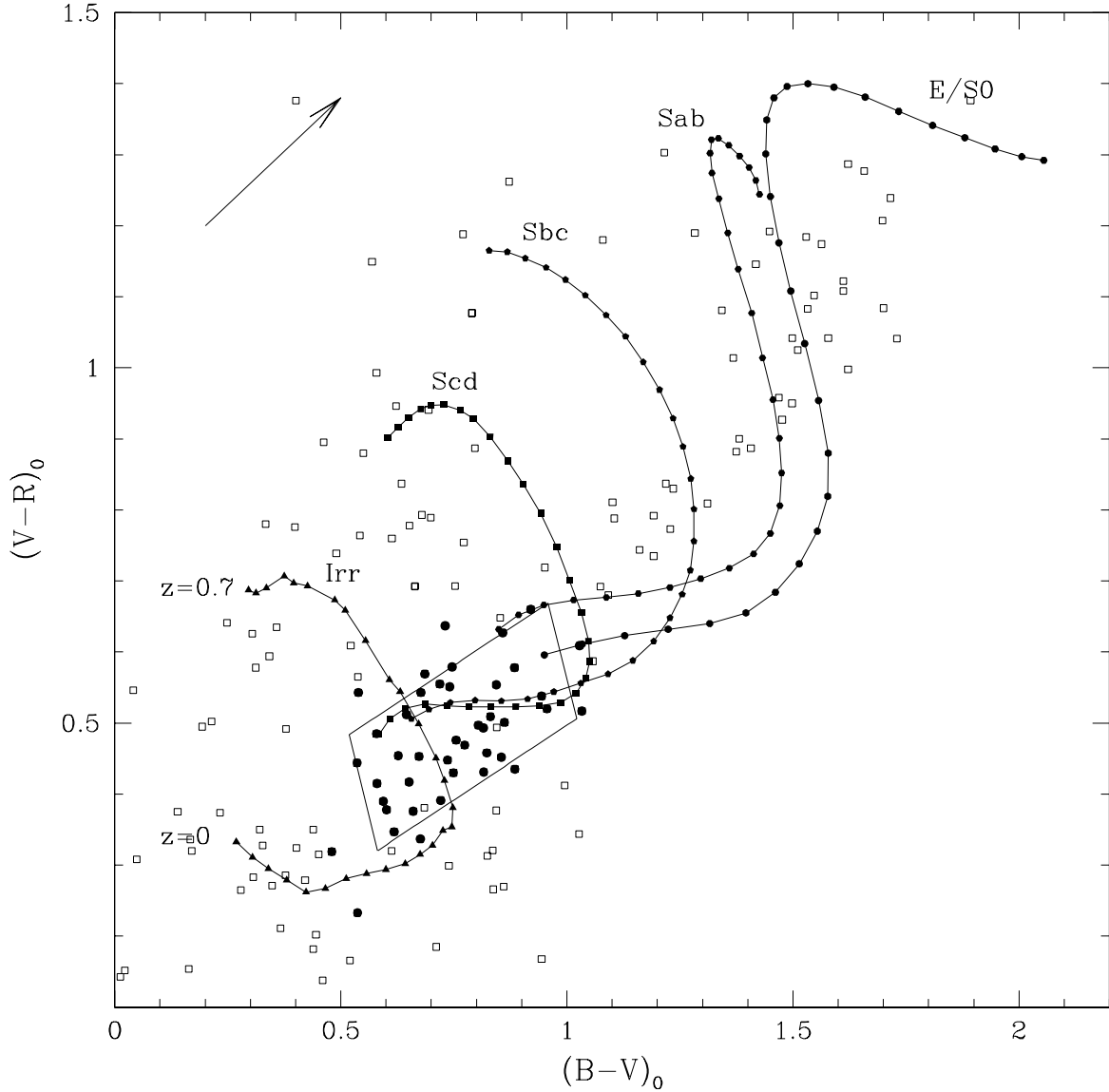


Fig. 2.— Color selection of GC candidates around NGC 7814. The colors of the 170 objects that appear as point sources in the WIYN images are shown here. Open squares are objects that failed to meet the magnitude/color selection criteria and filled circles are the final set of 42 GC candidates. For reference, the locations in the color-color plane of galaxies of various types are shown as tracks the galaxies would follow with increasing redshift. A reddening vector of length $A_V = 1$ magnitude appears in the upper left corner.

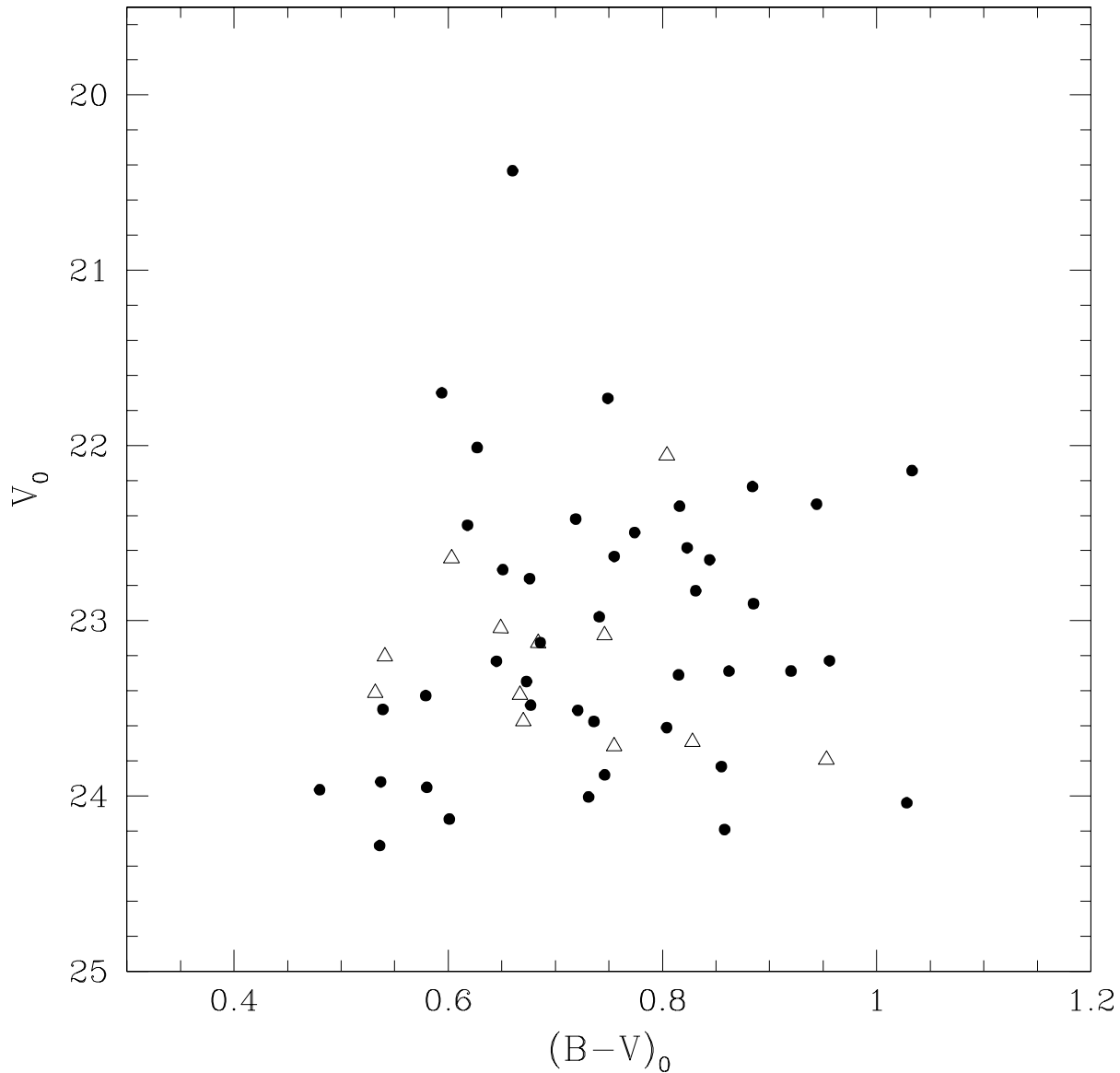


Fig. 3.— Color-magnitude diagram for GC candidates in NGC 7814. V versus $B - V$ is plotted for 54 GC candidates. Candidates detected in the HST images are shown as open triangles. Candidates from the WIYN images, or from both the HST and WIYN data, are shown as filled circles. Note that the magnitudes and colors have not been corrected for internal absorption in NGC 7814.

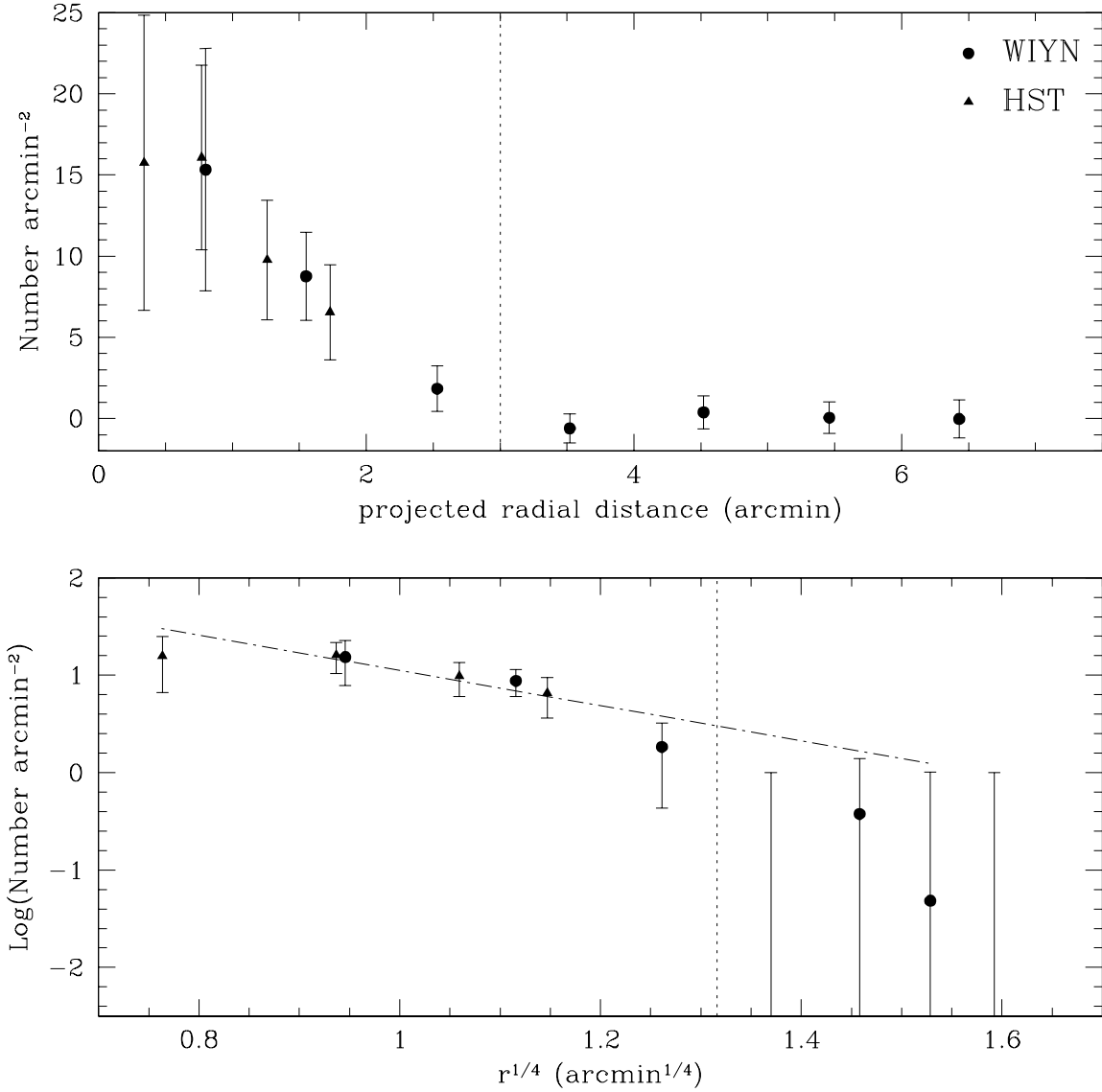


Fig. 4.— Radial distribution of GCs in NGC 7814. The top figure shows the surface density of GCs as a function of projected radial distance from the galaxy center. The bottom plot shows the log of the surface density versus $r^{1/4}$ and the dashed line is the best-fit deVaucouleurs profile. The vertical dotted line marks 3' in both plots, beyond which the GC surface density is consistent with zero within the errors. The data have been corrected for contamination, areal coverage, and magnitude incompleteness, as described in Section 4.1.

Table 1. Aperture Corrections
Used for Photometry of WIYN
Sources

Image	Aperture Correction
<i>B</i>	-0.223 ± 0.006
<i>V</i>	-0.179 ± 0.006
<i>R</i>	-0.230 ± 0.005

Note. — The values listed here are the difference between the total magnitude and the magnitude within an aperture of radius equal to the average FWHM of the image.

Table 2. Corrected Radial Profile for GCs in NGC 7814

Radius (arcmin)	Surface Density (arcmin $^{-2}$)
0.34	15.76 \pm 9.10
0.77	16.07 \pm 5.68
0.80	15.33 \pm 7.47
1.26	9.77 \pm 3.69
1.55	8.76 \pm 2.70
1.73	6.55 \pm 2.93
2.53	1.84 \pm 1.40
3.52	-0.61 \pm 0.90 [†]
4.52	0.38 \pm 1.02
5.46	0.05 \pm 0.96
6.43	-0.03 \pm 1.17 [†]

[†]A contamination correction has been applied to the surface density of GCs in each bin, resulting in a negative surface density in two of the outer bins.

Table 3. Total Numbers and Specific Frequencies for NGC 7814’s
GC System

$m - M$	Distance (Mpc)	M_V^T	N_{GC}	S_N	T
30.60	13.2	–20.40	140–190	1.0–1.3	1.9–2.5
30.95	15.5	–20.75	150–200	0.8–1.0	1.4–1.9